Elastic scattering spectroscopy for monitoring skin cancer transformation and therapy in the near infrared window

Kawthar Shurrab, Nabil Kochaji & Wesam Bachir

Lasers in Medical Science

ISSN 0268-8921

Lasers Med Sci
DOI 10.1007/s10103-019-02894-2

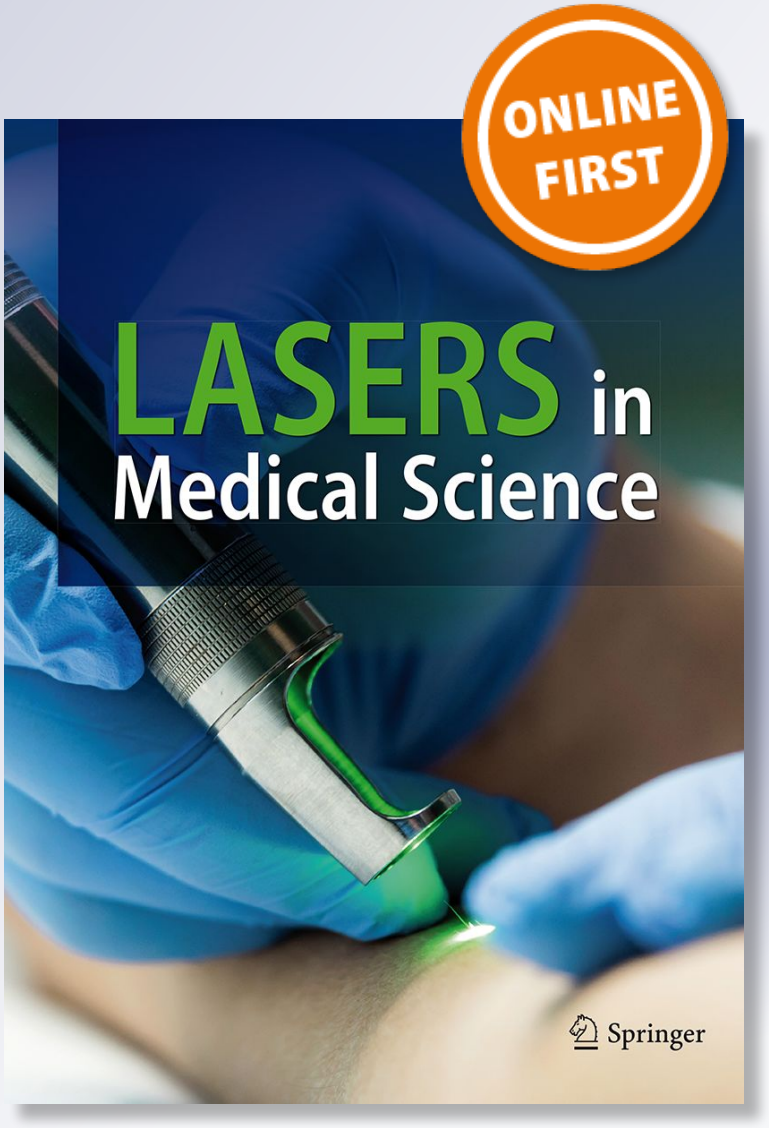

Springer

Lasers in Medical Science
https://doi.org/10.1007/s10103-019-02894-2

ORIGINAL ARTICLE

Elastic scattering spectroscopy for monitoring skin cancer transformation and therapy in the near infrared window

Kawthar Shurrab[1] · Nabil Kochaji[2] · Wesam Bachir[3,4]

Received: 1 August 2019 / Accepted: 26 September 2019

Abstract

There is a pressing need for monitoring cancerous tissue response to laser therapy. In this work, we evaluate the viability of elastic scattering spectroscopy (ESS) to monitor malignant transformations and effects of laser therapy of induced skin cancer in a hamster model. Skin tumors were induced in 35 mice, half of which were irradiated with 980 nm laser diode. Physiological and morphological transformations in the tumor were monitored over a period of 36 weeks using elastic scattering spectroscopy, in the near infrared window. Analytical model for light scattering was used to derive scattering optical properties for both transformed tissue and laser-treated cancer. The tissue scattering over the wavelength range (700–950 nm) decreased remarkably as the carcinogen-induced tissue transformed towards higher stages. Conversely, reduced scattering coefficient noticeably increased with increasing the number of laser irradiation sessions for the treated tumors. The relative changes in elastic scattering signal for transformed tissue were significantly different ($p < .05$). Elastic scattering signal intensity for laser-treated tissue was also significantly different ($p < .05$). Reduced scattering coefficient of treated tissue exhibited nearly 80% recovery of its normal skin value at the end of the experiment, and the treatment outcome could be improved by adjusting the number of sessions, which we can predict through spectroscopic optical feedback. This study demonstrates that ESS can quantitatively provide functional information that closely corresponds to the degree of pathologic transformation. ESS may well be a viable technique to optimize systemic melanoma and non-melanoma skin cancer treatment based on noninvasive tumor response.

Keywords Optical properties · Elastic scattering · Skin cancer · Diode laser · Spectroscopy

Introduction

To date, sustained and long-term recovery has been the main objective of most cancer treatments. Commonly used treatment methods such as radiation therapy and chemotherapy are used to decrease tumor size especially at advanced stages before surgical resection [1, 2]. This may allow full resection and function preservation. Nevertheless, patients do respond differently to these therapies. This may be attributed to differences in tissue functionality among individuals, which requires different treatment dosimetry [3]. An effective laser therapy can be related to reduction in tumor size, but this can take up to several months to observe [4]. On the other hand, tissue transformations in tumor functional and physical properties can be noticed well before changes in tumor shape are observed [5, 6].

Accordingly, a wide array of methods that are sensitive to these changes was devised to allow for early and effective treatment plan. Commonly used methods are positron emission tomography [7, 8], magnetic resonance imaging [9], and computed tomography [10, 11]. In fact, these modalities require the injection of contrast agents for accurate diagnosis. Moreover, contrast agents provide information about tumor vascular parameters such as blood flow and permeability that can be difficult to quantify accurately [12]. Alternatively,

We state that this is an original article that has not been previously published, and that it is not simultaneously under consideration by any other journal

✉ Kawthar Shurrab
Sh_kawther@yahoo.com

[1] Biomedical Photonics Laboratory, Higher Institute for Laser Research and Applications, Damascus University, Damascus, Syria

[2] Faculty of Dentistry, Al-Sham Private University, Damascus, Syria

[3] Biomedical Photonics Laboratory, Higher Institute for Laser Research and Applications, Damascus University, Damascus, Syria

[4] Faculty of Informatics Engineering, Al-Sham Private University, Al-Baramkeh, Damascus, Syria

Published online: 23 October 2019

optical techniques have shown great potential for monitoring laser therapy such as optical coherence tomography (OCT) which can potentially give a required diagnostic information eliminating the need for undesired biopsies that may cause pain, anxiety, and trauma to the patients [13]. In addition, quantitative analysis of OCT images has been investigated to differentiate biological tissue [14]. Recent research has focused on low-cost diffuse optical methods that are frequently used for diagnostic purposes as well [15]. These methods allow therapy outcome to be predicted as well as provide feedback to enhance tumor therapy. Also, optical techniques allow the extraction of inherent optical properties, mainly absorption and scattering coefficients, of living tissue. Tissue absorption contains information related to the concentration of biological chromophores, such as hemoglobin, water, lipids, and many others. This can be used to quantify physiological responses of treated tumors to laser therapy [16]. Also, the scattering parameters provide information about the structure and composition of tissue including cells and subcellular elements [17]. This information can indicate variation in physiological activities taking place in growing tumors and thus leads to increased scattering coefficient for the tumor. Therefore, optical diagnostic instrumentation can provide functional and structural information about tissue transformation before and after laser therapy [18, 19].

The aim of the present study is to investigate the efficacy of elastic scattering spectroscopy to monitor the scattering component of skin cancer response in the near infrared spectrum during cancer transformations and after treatment with 980 nm laser diode using a hamster model for induced skin cancer.

Materials and methods

Animal model

In this work, 35 hamsters (10–12 weeks of age) were used. They were kept in healthy conditions and at the laboratory temperature. A solution of 9, 10-dime thy 1-1, 2-benzanthracene (DMBA) was mainly used as a carcinogen solution in hamster skin [20, 21]. The area of interest on the skin was marked by a permanent ink pen to follow up the possible changes throughout the experiment. Specific solutions were applied topically on the back of hamster that is on the skin surface. A 980 nm Diode laser was used in a continuous mode with laser irradiation of 0.5 W, and the power density of the laser at the skin surface was 50 W/cm^2. The treatment fiber diameter was 200 μm. Laser irradiation was applied once a week, from the onset of tumor until the end of the experiment [22]. All hamsters were checked on a weekly basis, and monitored until spontaneous death, or were killed during the experiment.

Skin tissue sample was sandwiched between two glass microscope slides. The slides were cleaned with pure cellulose tissue that were wetted with isopropyl alcohol to get rid of any impurities or stains might be placed on the surface, and then immersing these slides in isopropyl alcohol for 1 min followed by a drying process with proper hot air.

All elastic scattering spectra were recorded at the same angle with reference to the surface of the slide and at the fixed distance from the sample, and then the scattering measurements were taken in the wavelength range of (400–1000 nm). The sources of uncertainties were maintaining stable, like (light, temperature, and humidity), and uncertainty were approximately ± 1%. The spectrum was measured in a dark room with ambient laboratory conditions. Also, the calibration procedures were used to normalize variability in the spectral response. The samples were fixed in formalin until the timing of spectroscopic measurements.

Elastic scattering spectroscopy

Spectroscopic measurements were conducted using a miniature fiber-based ESS system. Elastic scattering spectra were recorded ex vivo in the range of (400–1000) nm. A schematic description of the experimental setup is shown in Fig. 1. A broadband white light with a wavelength range of 400–1100 nm from a tungsten halogen lamp (Ocean Optics Inc., Dunedin, Florida, USA, HL-2000-HPFHSA) was delivered to the skin tissue of interest via an optical fiber located in a two-leg fiber optic probe (Ocean Optics Inc., Dunedin, Florida, USA). The HL-2000 light emission spectrum is given in Fig. 2.The core diameter of the probe is 200 μm with a numerical aperture of 0.22. The second leg of the optical fiber probe was used to collect and guide the back-reflected light emanated from the skin tissue underneath a miniature fiber optic spectrometer (Ocean Optics Inc., Dunedin, Florida, USA). The fiber optic-based spectrometer is connected to a

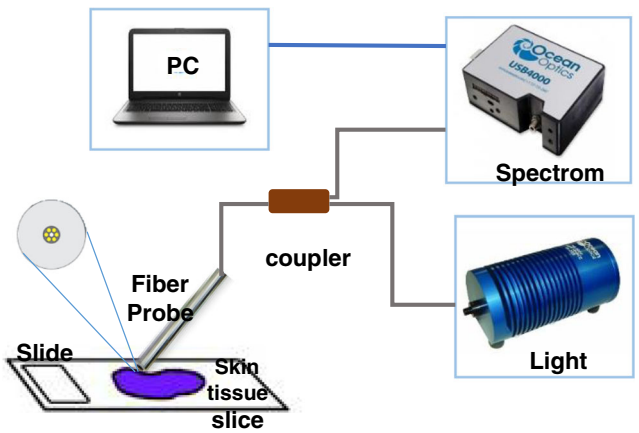

Fig. 1 Schematic illustration showing the elastic scattering optical setup. The system measures scattering spectrum of tissue slice through the use of a fiber optic bundle probe

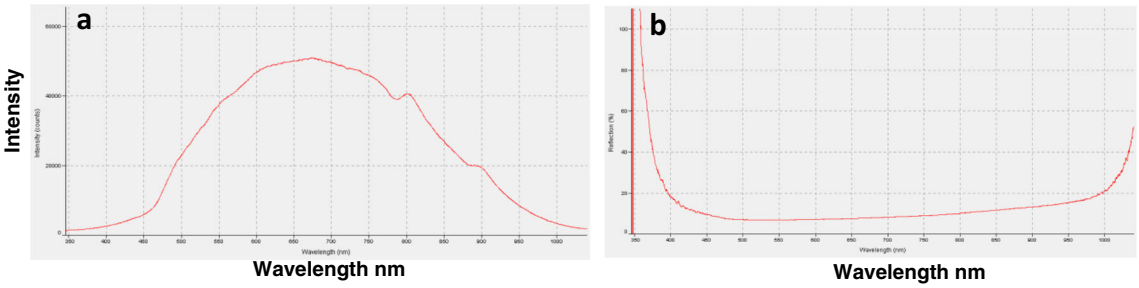

Fig. 2 **a** The spectrum of HL-2000 light source used in this work. **b** shows the ESS signal affected by the chromophores after carcinogens at 32 weeks

laptop for data acquisition and spectral analysis of recordings. The portable spectrometer has a 600 lines/mm, together with a 200-μm slit and a 500-nm blazed grating capable of operating in the 345- to 1080-nm wavelength range. Additionally, the compact spectrometer is equipped with a 3648 element CCD array detector. Spectra Suite software (Ocean Optics Inc., USA, version 2011) was utilized to acquire the spectra in the visible and near infrared regions. Calibration of measurement, dark current, and background measurements were carried out at the same setting before each session. To further improve the signal to noise ration of the recorded signals, the acquired spectra were averaged, smoothed, and had an integration time of 25 min.

Figure 2a shows the spectrum of light source in the whole spectrum region of ESS and Fig. 2b shows how far the visible spectrum is affected by the chromophores after carcinogen at 32 weeks.

Spectral analysis

Elastic scattering spectra were recorded five times for each sample from different locations in the treated or investigated area. Consequently, spectral analysis was performed in the near-infrared range from 700 to 950 nm in order to minimize the possible contribution of unwanted major chromophores in skin slice such as hemoglobin and melanin. Elastic scattering signal recorded is assumed to be mainly dependent on scattering contribution of biological tissue. Thus, all other absorptive contribution to the signal can be neglected especially in the investigated wavelength range from 700 to 950 nm. The main scattering parameter is the reduced scattering coefficient μ_s'. The scattering slope is related to the size of skin structures. Often, the emanated scattering spectrum is a combination of two types of elastic scattering skin tissue, that is, Mie and Rayleigh scattering. Spectral data were interpreted based on analytical model of light scattering in biological tissue reported by Jacques [23] given by

$$\mu_s'(\lambda) = a'\left(f_{Ray}\left(\frac{\lambda}{500(nm)}\right)^{-4} + \left(1-f_{Ray}\right)\left(\frac{\lambda}{500(nm)}\right)^{-b_{Mie}}\right) \quad (1)$$

where a is the scattering magnitude (cm^{-1}) and b is the dimensionless scattering power. In this expression, the scattering is described in terms of the Rayleigh scattering, $a'\,f_{Ray}(\lambda/500\ nm)^{-4}$, and the Mie scattering, $a'\,(1-f_{Ray})(\lambda/500\ nm)^{-b}{}_{Mie}$, at λ certain reference wavelength, 500 nm. The factor a' equals $\mu_s'(\lambda = 500\ nm)$. Jacques [23] also found that the above equation could be reduced to more compact form expressed by

$$\mu_s' = a\left(\frac{\lambda}{800(nm)}\right)^{-b}, \quad (2)$$

Since scattering properties exhibit a simple λ^{-b} behavior. According to measurement made by Jacques, equation (2) is reasonably sufficient to characterize the behavior of different groups of tissues such as skin tissue. The equations are equally good for prediction of tissue scattering within the 400–1300 nm wavelength range. But outside this range in either the ultraviolet or the longer infrared, the two equations diverge. Thus, Eq. (2) is sufficient and valid in the range from 700 to 950 nm. The reference wavelength at 500 nm given in the original equation is replaced with 800 nm to correspond to the NIR range of wavelength used in this study.

Inverse model approach deals with the process of extracting the model parameters from the data collected experimentally. Hence, the parameters extracted represent the function of the biological system.

Most of these approaches are fundamentally based on using the solution of the forward model to generate a spectrum, and the model parameters are updated to match the generated spectrum to the measured spectrum. When a close fit to the simulated spectrum is found, the parameters (underlying optical properties) of the simulated spectrum form the starting point to adjust the parameters in order to obtain a best fit.

A linear regression model was used to examine the elastic scattering spectrum in the defined range of wavelength. Spectral analysis was carried out using Matlab 2015 (Mathworks.com, 2015b, USA). Then, the parameters of tissue scattering model were computed by inverse algorithm. The flowchart of inverse algorithm is shown in Fig. 3.

In this algorithm, initial scattering parameters: scattering magnitude, scattering power, and reference wavelength are given in order to generate the corresponding forward model.

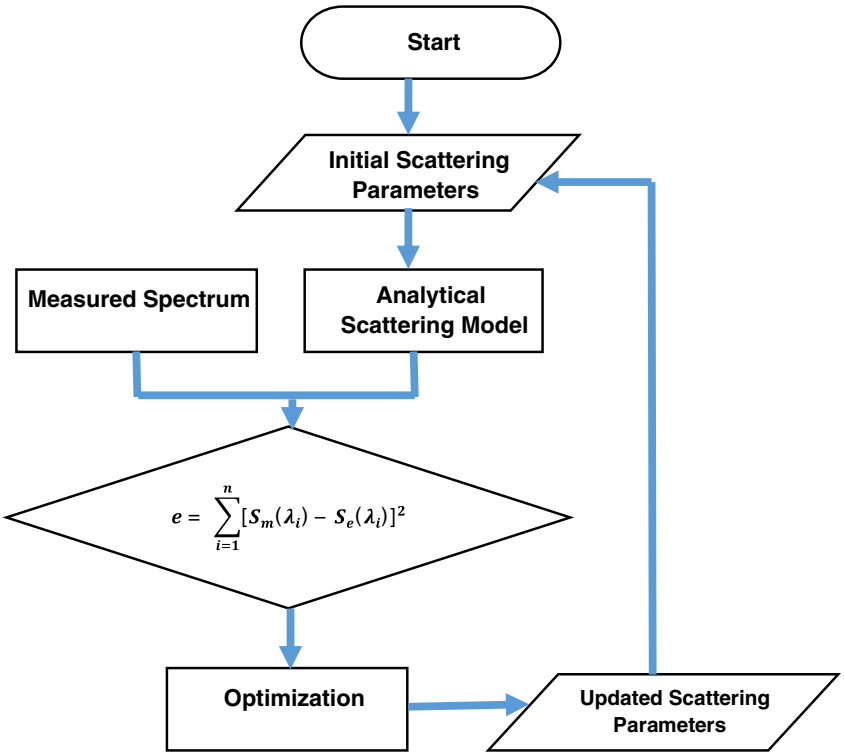

Fig. 3 Flowchart of the inverse model for fitting the measured scattering spectrum to the analytical scattering model

The forward model spectra generated (by updating the model scattering parameters) are compared to the measured spectra, and an error function is defined. The inverse method in this work uses the least squares error to compute the minimum error function followed by an update of the model parameters on error function value.

As a result, the parameters of the model at which the sum of the squared residuals is minimized are referred to as the best fit. The nonlinear least squares error method is considered in models where the forward model is a nonlinear function of model parameters. In our system, the forward model of light transport has a nonlinear dependence on the model parameters.

Figure 3 shows the flowchart of the algorithm used for extracting the scattering properties of the measured spectra, that is, transformed tissue and treated tumor tissue samples. When a best fit is obtained based on the value of error function, the inverse process is terminated and the final parameters of the model are defined to be the output parameters.

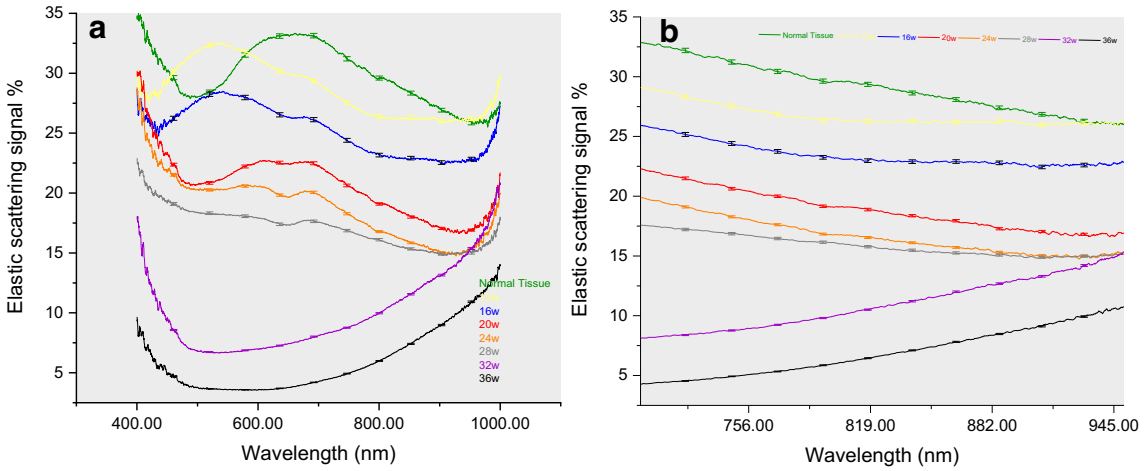

Fig. 4 Mean and standard deviation of elastic scattering spectra obtained from skin samples. Lines represent normal tissue spectrum and seven stages of cancer transformation starting from 12 to 36 weeks. **a** Over the entire range of wavelength (400–1080 nm). **b** Over the NIR range of wavelength (700–950 nm)

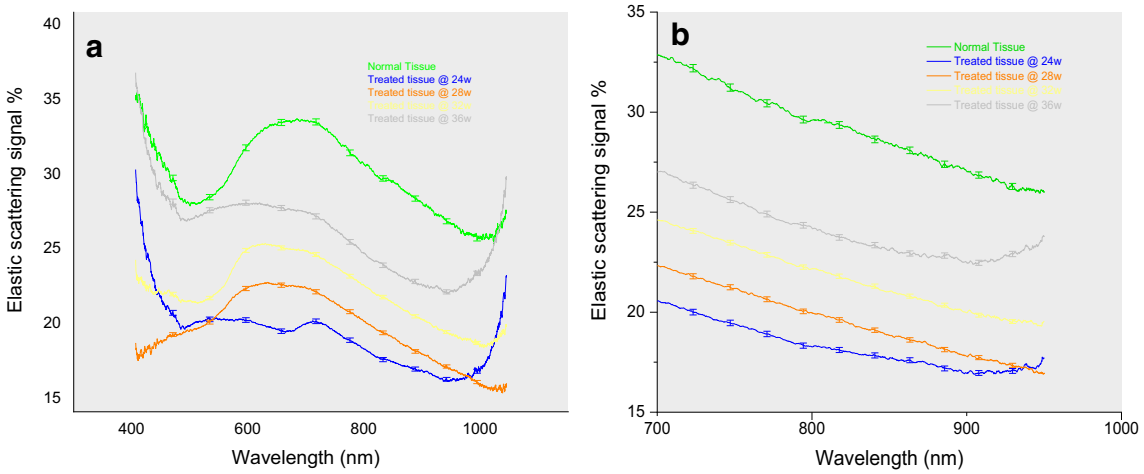

Fig. 5 Mean and standard deviation of elastic scattering spectra obtained from skin samples. Lines represent normal tissue spectrum and skin tissue spectra after treatment. **a** Over the entire range of wavelength (400–1080 nm). **b** Over the NIR range of wavelength (700–950 nm)

Variation in scattering parameters between control group and treated tissue groups were examined using nonparametric ANOVA analysis. Significance level was set at $p \leq 0.05$. Similarly, nonparametric ANOVA was used to examine the scattering coefficient variation between control group and cancer-induced tissue samples.

Results

Mean values and standard deviation of elastic scattering spectra for normal tissue sample and different stages following the application of carcinogen are shown in Fig. 4a. Skin tissue transformations due to the carcinogen can be noticed over the entire follow-up period of 36 weeks. It can be noticed that the most pronounced difference between spectra is in the NIR window, that is, from 700 to 1000 nm.

It is noteworthy to say that the peak wavelength shift can be attributed to the variation in optical properties of the samples due to thermal effect of laser radiation. Another factor that may contribute to this shift is the presence of impurities and possibly remnants of chromophores in the tissue samples. Thus, the focus of this study was on the NIR window.

Figure 4b shows the spectroscopic recordings from 700 to 950 nm. All spectra exhibit characteristic decline over the defined range of wavelength.

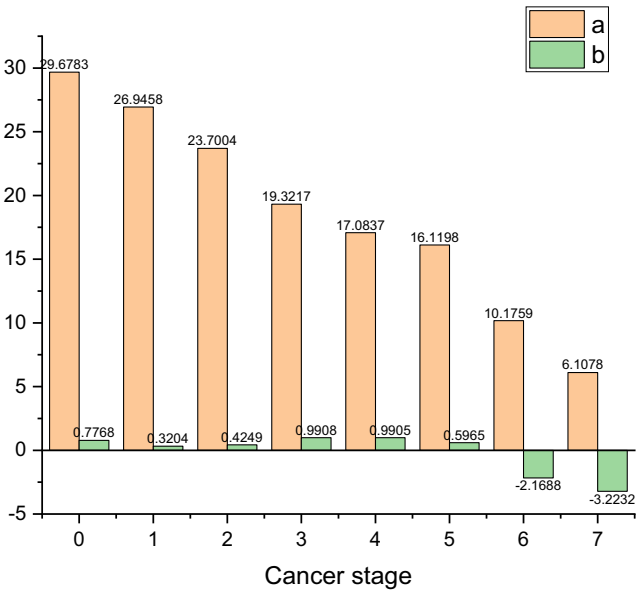

Fig. 6 Optical scattering parameters (**a**, **b**) extracted from elastic scattering spectra of normal tissue denoted by 0 and seven stages of tissue transformation represented by numbers from 1 to 7 respectively using inverse analytical model

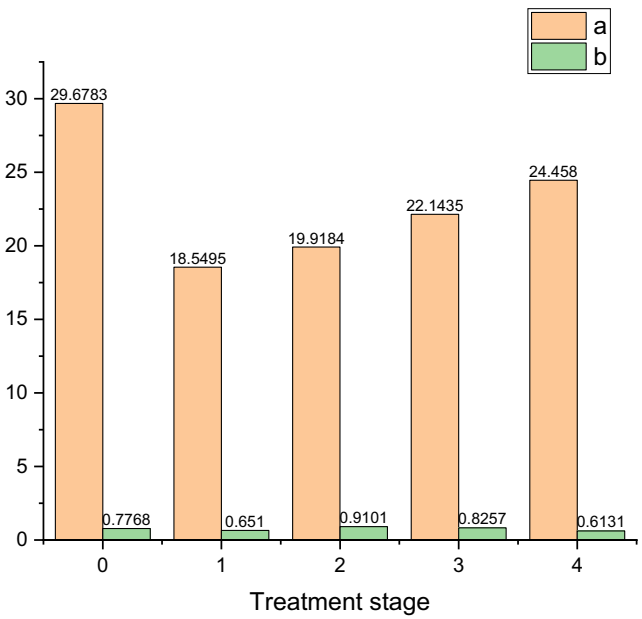

Fig. 7 Optical scattering parameters (**a**, **b**) extracted from elastic scattering spectra of normal tissue denoted by 0 and four stages of treated tumor tissue represented by numbers from 1 to 4 respectively using inverse analytical model

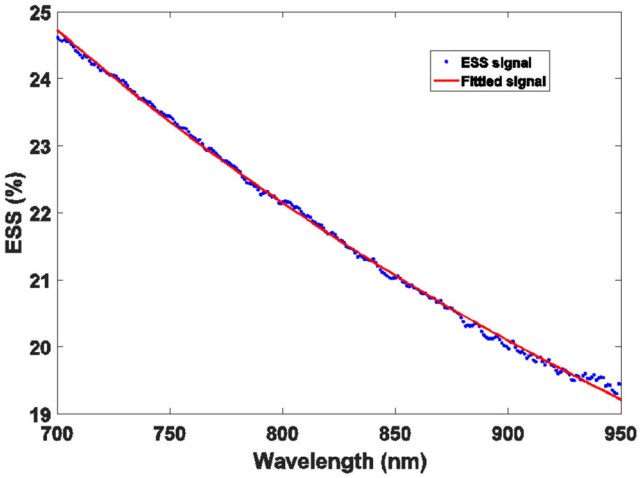

Fig. 8 Reconstruction of the measured scattering spectrum at week 32

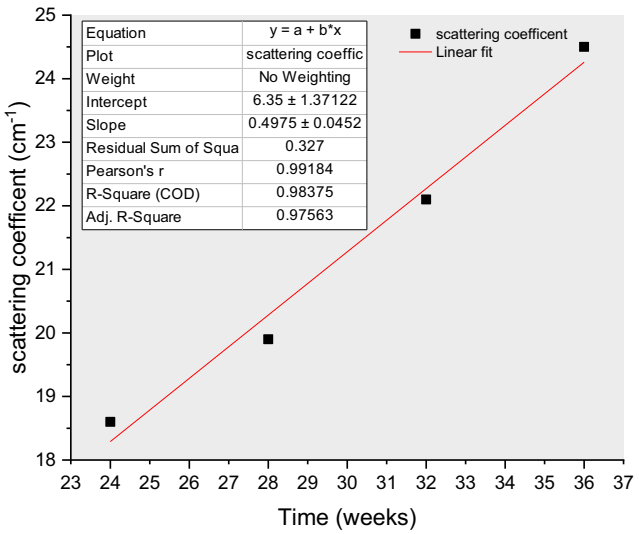

Fig. 10 Reduced scattering coefficient as a function of the length of laser treatment period

Scattering signals showed an increased intensity following laser application starting from 20 weeks until the end of the experiment, indicating an improvement in skin tissue as shown in Fig. 5a.

Reduced scattering coefficient of treated tissue exhibited nearly 80% recovery of its normal skin value at the end of the experiment. Figure 5b shows the spectroscopic recordings of healthy tissue and skin after laser treatment over the NIR range of wavelength (700–950 nm).

A significant difference ($p < 0.05$) in the elastic scattering coefficients was found between samples tested for both transformed tissue and treated tissue groups.

The scattering magnitude, which is given in Eq. 2 and obtained from inverse algorithm model, shows a decrease with increasing cancer transformation stage as shown in Fig. 6 and returns to its original value after laser treatment as depicted in Fig. 7. Whereas, scattering power value b is inconsistently changed. Therefore, only the scattering parameter a can be relied on for evaluation of cancer transformation and treatment.

Reconstruction of the measured scattering spectrum was performed using linear regression model. Figure 8 shows an example of fitting of the reconstructed spectrum and the measured spectrum in week 32 after carcinogens.

Discussion

Generally, in the NIR window, the absorption of hemoglobin and other chromophores such as melanin and water are minimized. To justify the use of this limited number of wavelengths, we recorded the full spectrum from 400 to 1000, which is the full range of our spectrometer, then the visible range from our measurements was excluded because it was noticed that the changes in ESS signal from 400 to 700 nm were unstable due to contributions of different chromophores. Besides, the range from 700 to 950 was advised in this study to be maximum at 950 in order to avoid unreliable recordings at the end of the available bandwidth of the spectrometer.

The results presented in this work show that elastic scattering spectroscopy is able of investigating the effect on DMBA-induced carcinogen on transformations in skin cancer. Trends in scattering parameters were examined over a period of 1 month. Variation of reduced scattering coefficient with increasing the stage of tissue transformation is in accord with previous research, such as the work of Rajaram et al. [24, 25], Lim et al. [26], and Sharma et al. [27]. In their studies, lower

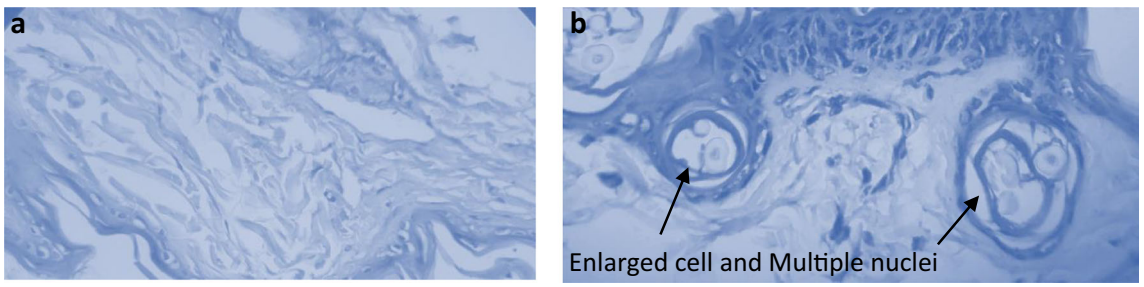

Fig. 9 **a** Histological appearance of hamster normal skin. With normal nuclei, **b** cancer skin tissue reveals increased size and nuclei concentration. Irregular cells and more than two nuclei within the cell. Black arrows point to increase the nuclei

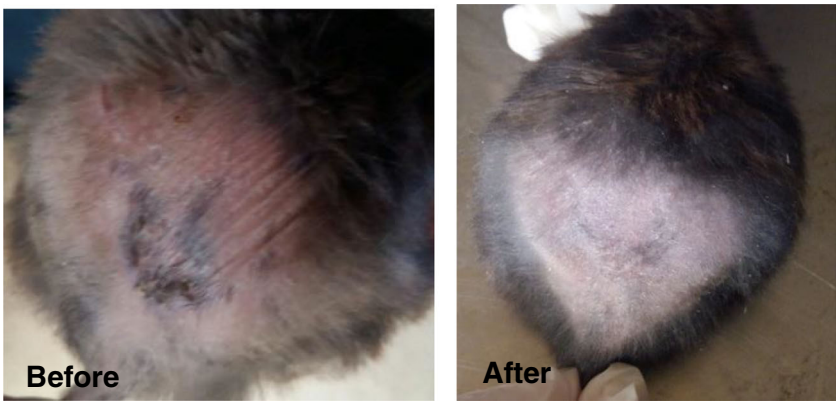

Fig. 11 Before and after laser treatment

values of reduced scattering coefficient are noticed with increasing the transformation stage towards high-grade cancer.

It is noteworthy to say that the in the last two spectra at 32 and 36 weeks in Fig. 5, the intensity of light increased with increasing wavelength; this can be explained by the fact that the optical path length of final signal of scattered photons is shorter than diffused photon paths in tissue. In addition, the nuclei concentration and size are increased within cancer tissue, which may affect spectral slope, as shown in histological image in Fig. 9a, b.

The observed decline in scattering parameter **a** with increasing cancer transformation stage indicates lower scattering. This could be attributed to the increase in nuclei concentration within cancerous tissues (e.g., formation of multiple nuclei). Also, this could be explained by light scattering on cellular microstructures that are changed and becoming more condensed towards cancer. In contrast, Scattering parameter *a* increased after treatment.

Another important finding is that the reduced scattering coefficient can reliably be adopted as an optical characteristic parameter for discriminating the morphology and function of the cancerous/treated regions thus defining the stage of tissue transformation in both forward and backward direction corresponding to malignancy and normality, respectively.

In addition, our findings reveal a close relationship between the laser treatment period and the reduced scattering coefficient as shown in Fig. 10. Thus, the number of laser treatment sessions required for restoring normal reduced scattering coefficient value can be predicted. In other words, laser treatment plan and dosimetry can be adjusted accordingly.

It may be possible to use the information and results gained from this study to optimize the dose and adjust the laser therapy protocol for each specific tumor based on the optical feedback provided by optical spectroscopic modality. Boone et al. [28] report the use of promising optical imaging known as optical coherence tomography for differentiating benign skin lesions from malignant ones. However, the presented low-cost and portable elastic scattering spectroscopic technique in this work allows sharp differentiation between normal and cancerous skin regions.

The results demonstrated that the ESS parameters in the treated hamsters differed significantly from the untreated cancer-induced hamsters.

A clear understanding of the origins of the optical properties in terms of elastic scattering could provide more physiological information leading to an improved *in vivo* tissue treatment and dosimetry.

For comparison, an illustration of the clinical difference before and after laser treatment at week 36 at the end of the experiment can be seen in Fig. 11 [29]. This difference has been emphasized clearly in ESS measurements as mentioned above.

Conclusion

Our findings indicate that the reduced scattering coefficient decreased as the carcinogen tissue transformed towards higher stages. Conversely, it has been noticeably increased during therapy. Thus, the reduced scattering coefficient can predict the number of laser irradiation sessions required for tumor treatment through spectroscopic optical feedback; thus, the normal values of scattering coefficient can be retrieved.

Future works should focus more on the histopathology combined with elastic scattering spectroscopy, to provide better understanding of all variations in the spectra. This may highly improve the sensitivity of early detection to any small transformation might be caused by cancer and potentially lead to the application of ESS in clinical oncology where the extracted parameters are directly clinically relevant to functional physiology of biological tissue of interest. Being noninvasive and portable, elastic scattering spectroscopy is expected to provide a prediction of the therapy response of tumors to laser therapy. This would result in higher survival rates for patients and considerable reduction in healthcare costs.

Acknowledgments The authors gratefully acknowledge extend their gratitude to all colleagues at Damascus University and Higher Institute for Laser Research and Applications who cooperated in this study.

Compliance with ethical standards

Conflict of interest The authors declare that they have no conflict of interest.

Ethical approval All procedures were approved by institutional ethical, according to Damascus University ethical committee decision no. 3164

References

1. McCarthy K, Pearson K, Fulton R, Hewitt J (2012) Pre-operative chemoradiation for non-metastatic locally advanced rectal cancer. Cochrane Database Syst Rev 12:CD008368
2. Rydzewska L, Tierney J, Vale CL, Symonds PR (2012) Neoadjuvant chemotherapy plus surgery versus surgery for cervical cancer. Cochrane Database Syst Rev 12:CD007406
3. Ueda S, Roblyer D, Cerussi A et al (2012) Baseline tumor oxygen saturation correlates with a pathologic complete response in breast cancer patients undergoing neoadjuvant chemotherapy. Cancer Res 72:4318–4328
4. Garland ML, Vather R, Bunkley N et al (2014) Clinical tumour size and nodal status predict pathologic complete response following neoadjuvant chemoradiotherapy for rectal cancer. Int J Color Dis 29:301–307
5. Jiang S, Pogue BW, Kaufman PA et al (2014) Predicting breast tumor response to neoadjuvant chemotherapy with diffuse optical spectroscopic tomography prior to treatment. Clin Cancer Res 20: 6006–6015
6. Vaupel P, Kallinowski F, Okunieff P (1989) Blood flow, oxygen and nutrient supply, and metabolic microenvironment of human tumors: a review. Cancer Res 49:6449–6465
7. Lehtio K, Eskola O, Viljanen T et al (2004) Imaging perfusion and hypoxia with PET to predict radiotherapy response in head-and-neck cancer. Int J Radiat Oncol Biol Phys 59:971–982
8. Jacobson O, Chen X (2013) Interrogating tumor metabolism and tumor microenvironments using molecular positron emission tomography imaging. Theranostic approaches to improve therapeutics. Pharmacol Rev 65:1214–1256
9. DeVries AF, Kremser C, Hein PA et al (2003) Tumor microcirculation and diffusion predict therapy outcome for primary rectal carcinoma. Int J Radiat Oncol Biol Phys 56:958–965
10. Hermans R, Lambin P, Van der Goten A et al (1999) Tumoural perfusion as measured by dynamic computed tomography in head and neck carcinoma. Radiother Oncol 53:105–111
11. Preda L, Calloni SF, Moscatelli ME et al (2014) Role of CT perfusion in monitoring and prediction of response to therapy of head and neck squamous cell carcinoma. Biomed Res Int 2014:917150
12. Anderson H, Price P, Blomley M et al (2001) Measuring changes in human tumour vasculature in response to therapy using functional imaging techniques. Br J Cancer 85:1085–1093
13. Turani Z, Fatemizadeh E, Blumetti T, et al (2019) Optical radiomic signatures derived from optical coherence tomography images improve identification of melanoma. Cancer Res 79(8):2021-2030
14. Avanaki MRN, Podoleanu AG, Schofield JB, Jones C, Sira M, Liu Y, Hojjat A (2013) Quantitative evaluation of scattering in optical coherence tomography skin images using the extended Huygens–Fresnel theorem. Appl Opt 52:1574–1580
15. Hafez R, Hamadah O, Bachir W (2015) Mapping of healthy oral mucosal tissue using diffuse reflectance spectroscopy: ratiometric-based total hemoglobin comparative study. Lasers Med Sci 30:2135 https://doi.org/10.1007/s10103-015-1765-y
16. Mourant JR, Freyer JP, Hielscher AH et al (1998) Mechanisms of light scattering from biological cells relevant to noninvasive optical-tissue diagnostics. Appl Opt 37:3586–3593
17. Mourant JR, Fuselier T, Boyer J et al (1997) Predictions and measurements of scattering and absorption over broad wavelength ranges in tissue phantoms. Appl Opt 36:949–957
18. Cheung C, Culver JP, Takahashi K et al (2001) In vivo cerebrovascular measurement combining diffuse near-infrared absorption and correlation spectroscopies. Phys Med Biol 46:2053–2065
19. Laughney AM, Krishnaswamy V, Rizzo EJ et al (2012) Scatter spectroscopic imaging distinguishes between breast pathologies in tissues relevant to surgical margin assessment. Clin Cancer Res 18: 6315–6325
20. Sugimura T (1986) Studies on environmental chemical carcinogenesis in Japan. Science 233:312 Academic OneFile
21. SHubik P, Pietra G, Dellaporta G (1960) Studies of skin carcinogenesis in the Syrian golden hamster. Cancer Res 20:100–105
22. Shurrab K, Kochaji N, Bachir W (2017) Development of temperature distribution and light propagation model in biological tissue irradiated by 980 nm laser diode and using COMSOL simulation. J Laser Med Sci 8(3):118–122
23. Jacques SL (2013) Optical properties of biological tissues: a review. Phys Med Biol 58(11):R37–R61. https://doi.org/10.1088/0031-9155/58/11/r37
24. Rajaram N, Aramil TJ, Lee K, Reichenberg JS, Nguyen TH, Tunnell JW (2010) Design and validation of a clinical instrument for spectral diagnosis of cutaneous malignancy. Appl Opt 49(2): 142–152
25. Rajaram N, Reichenberg JS, Migden MR, Nguyen TH, Tunnell JW (2010) Pilot clinical study for quantitative spectral diagnosis of non-melanoma skin cancer. Lasers Surg Med 42(10):716–727
26. Lim L, Nichols B, Migden MR, Rajaram N, Reichenberg JS, Markey MK, Ross MI, Tunnell JW (2014) Clinical study of non-invasive in vivo melanoma and nonmelanoma skin cancers using multimodal spectral diagnosis. J Biomed Opt 19:117003
27. Sharma M, Marple E, Reichenberg J, Tunnell JW (2014) Design and characterization of a novel multimodal fiber-optic probe and spectroscopy system for skin cancer applications. Rev Sci Instrum 85:083101
28. Boone MALM, Suppa M, Dhaenens F et al (2016) In vivo assessment of optical properties of melanocytic skin lesions and differentiation of melanoma from non-malignant lesions by high-definition optical coherence tomography. Arch Dermatol Res 308:7. https://doi.org/10.1007/s00403-015-1608-5
29. Shurrab K, Kochaji N, Bachir W (2019) Effect of laser irradiation on the progression of skin cancer using carcinogen among hamsters. Iran J Med Phys 16(4):314–318